

Highly nonlinear optical regime in graphene-assisted cavities: lasing threshold bares graphene nonlinearity

Alessandro Ciattoni¹ and Carlo Rizza^{2,1}

¹*Consiglio Nazionale delle Ricerche, CNR-SPIN, 67100 Coppito L'Aquila, Italy*

²*Dipartimento di Scienza e Alta Tecnologia, Università dell'Insubria, 22100 Como, Italy*

Strong nonlinear optical mechanisms operating in a miniaturized environment have a key role in photonics since they allow complex and versatile light manipulation within subwavelength devices. On the other hand, due to its two-dimensional planar geometry, graphene can easily be embedded within miniaturized structures and has fascinating linear and nonlinear optical properties arising from its relativistic electron dynamics. However, very few light steering graphene-based setups with a strong nonlinear behavior have been proposed since, due to its intrinsic planar localization, graphene nonlinearity has to be exploited through novel schemes not available in standard bulk nonlinear optics. Here we show that an active cavity hosting a graphene sheet, when tuned near its lasing threshold, is able to isolate the spatially localized graphene nonlinearity thus producing a very strong nonlinear device response with multi-valued features. The proposed strategy for exploiting graphene nonlinearity through its baring could open novel routes for conceiving ultra-efficient nonlinear photonic devices.

Achieving versatile and externally driven light manipulation at chip-scale is a basic task of modern photonics since it would provide those optoelectronic circuit components (e.g. optical transistors, logic gates, etc.) required for devising a novel generation of ultra-high speed computing devices. After its efficient production through exfoliation, graphene has soon been identified as an excellent optoelectronic material [1, 2] since the Dirac cone characterizing its electronic band structures provides a large carrier mobility yielding broadband and very efficient light-coupling [3]. Besides chemical potential strongly affects graphene electron dynamics so that the optical response can be both structurally designed through chemical doping and rapidly driven through ex-

ternally applied bias voltages. Accordingly a number of graphene-based devices have been proposed as polarizers [4–6], optical modulators [7–10], photodetectors [11–14], saturable absorbers and mode-locked ultrafast lasers [15–17]. In addition, the linear band structure provides graphene a large and broadband Kerr-like optical nonlinearity since at each photon frequency there is an available interband optical transition [18–23]. Accordingly, a number of remarkable effects due to such pronounced nonlinearity have been considered such as efficient third harmonic generation [24], nonlinear surface plasmons propagation [25], propagation of nonlinear modes through dielectric waveguides hosting graphene sheets [26] and nonlinear optical propagation in graphene-clad tapered fibers [27].

Even though remarkable such achievements have the common drawback of requiring relatively large optical powers as a consequence of the absolute smallness of the graphene nonlinear susceptibility (which is yet much larger than that of insulating materials [20]). Therefore, as in standard nonlinear optics without graphene, a field enhancement mechanism has to support the graphene-based nonlinear setup for triggering a low-intensity strong nonlinear optical regime. Recently strong field enhancement effects have been considered in the presence of graphene [28, 29]. However, to the best of our knowledge, achieving feasible (low-intensity) nonlinear light steering by combining graphene optical nonlinearity with a field enhancement mechanism has been shown in a very single paper by Gu *et al.* [30] where the authors show that placing a graphene sheet on the top of a silicon photonic crystal hosting a high-Q cavity (responsible for a large in-cavity field enhancement) produces optical bistability, self induced regenerative oscillations and coherent four-wave mixing accessible at ultra-low optical intensities.

In this paper, we show that a graphene sheet, placed within an active cavity tuned near its lasing threshold, turns the linear cavity behavior into a very highly nonlinear one, transmissivity and reflectivity being multi-

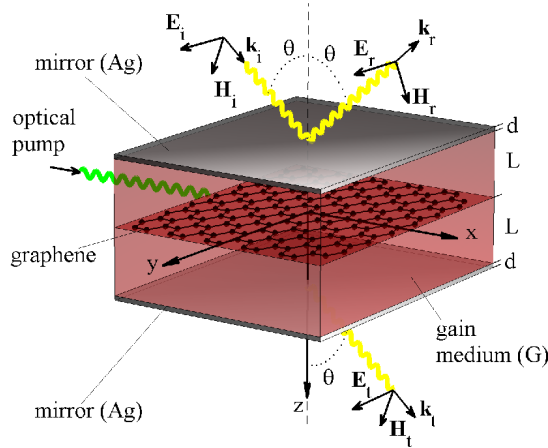


FIG. 1: **Graphene-assisted cavity geometry.** Geometry of the graphene layer embedded within a gain medium (G) enclosed by two metallic (Ag) mirrors. The cavity is illuminated by an inclined monochromatic wave (i) which produces reflected (r) and transmitted waves (t). The cavity is also illuminated by an inverting pump beam.

valued functions of both optical intensity and graphene chemical potential. Recently it has been proposed to use graphene sheets within passive optical cavities for achieving improved matter-radiation control [31, 32]. Here we consider a novel mechanism where the cavity at its lasing threshold literally bares the graphene nonlinearity since, in this situation, the field replication after a round trip inside the cavity amounts to a linear propagation compensation which, in turn, leaves graphene nonlinearity as the main agent ruling the cavity behavior. Generally, harnessing graphene nonlinearity in a bulk device is hampered by its intrinsic planar localization whereas the strategy discussed in this paper overcomes the difficulty just exploiting such localization. Since the proposed mechanism operates at ultra-low optical intensities and it is supported by a very simple setup we believe it can pave the way for the devising a novel generation of compact nonlinear light-steering devices.

I. RESULTS

Graphene-assisted cavity optical response. In Fig.1, the graphene assisted cavity is sketched together with the geometry of the interacting electromagnetic field. The graphene sheet is embedded between two layers (G) of thickness L filled by a gain medium (e.g. a dye-doped polymer) enclosed by two metallic mirrors (Ag) of thickness d . The cavity is excited by a monochromatic inclined TE-polarized plane wave (i) producing reflected (r) and transmitted (t) fields. In our analysis we neglect the gain nonlinearity by self-consistently assuming the optical intensity within the bulk to be much smaller than the gain saturation intensity. As a consequence, propagation of laser radiation within the active medium (and through the mirrors) is purely linear, the free cavity (without graphene) being a standard linear optical device. Due to the extremely small thickness of the graphene layer, we model its effect through the matching conditions $E_y^+ - E_y^- = 0$ and $H_x^+ - H_x^- = K_y$ i.e. the continuity of the electric field tangential component and the discontinuity of the magnetic field tangential component produced by the graphene surface current [19]

$$K_y = \sigma_1 E_y + \frac{3}{4} \sigma_3 |E_y|^2 E_y \quad (1)$$

where $E_y = E_y^+ = E_y^-$. Here the nonlinear corrections to the surface current have been taken into account up to the first order and the effect of higher harmonics generation have been neglected (see Methods). Both the linear surface conductivity σ_1 and its nonlinear correction σ_3 are strongly affected by the graphene chemical potential thus providing the system an overall tunability through chemical doping and electrical gating. Exploiting the spatial localization of the graphene nonlinearity

it is simple to obtain the equation (see Methods)

$$\left[\frac{3}{8} |\Lambda|^2 \sqrt{\frac{\mu_0}{\epsilon_0}} \sigma_3 |E_t|^2 + \left(\frac{\Omega}{\Lambda} + \frac{1}{2} c \mu_0 \sigma_1 \right) \right] E_t = \frac{\cos \theta}{\Lambda^2} E_i \quad (2)$$

joining the amplitudes E_i and E_t of the incident and transmitted waves, respectively. Here Ω and Λ are dimensionless complex factors depending on the radiation frequency, the inclination angle θ , and the gain medium and mirrors' slabs thicknesses and dielectric permittivities, ϵ_G and ϵ_{Ag} . Note that, if the nonlinear contribution to the surface current of Eq.(1) is negligible ($\sigma_3 = 0$), Eq.(2) yields

$$\frac{|E_t|^2}{|E_i|^2} = \frac{\cos^2 \theta}{|\Lambda|^4 \left| \frac{\Omega}{\Lambda} + \frac{1}{2} c \mu_0 \sigma_1 \right|^2} \quad (3)$$

which is the transmittance function of the linear cavity.

Mechanism supporting the strong nonlinear regime. In order to investigate the transmittance $T = |E_t|^2/|E_i|^2$ of the graphene-assisted cavity, it is convenient to introduce the dimensionless quantities

$$\begin{aligned} \tilde{T} &= \left(\frac{3|\Lambda|^4}{8 \cos \theta} c \mu_0 |\sigma_3| |E_i|^2 \right)^{2/3} T, \\ W &= \frac{|\sigma_3|}{\sigma_3} \frac{2|\Lambda|^{2/3} \left(\frac{\Omega}{\Lambda} + \frac{1}{2} c \mu_0 \sigma_1 \right)}{(3 \cos^2 \theta c \mu_0 |\sigma_3| |E_i|^2)^{1/3}} \end{aligned} \quad (4)$$

since Eq.(2), after taking the square modulus of both its member, yields

$$|\tilde{T} + W|^2 \tilde{T} = 1. \quad (5)$$

This is a simple and very general equation whose overall dependence on the specific device and excitation physical parameters has been fully absorbed in the parametrization of Eqs.(4). Here \tilde{T} is a real quantity proportional to the transmittance T and W is a complex parameter depending on the whole system status and excitation. In Fig.2a we plot the surface \tilde{T} on the complex plane W as evaluated from Eq.(5) and we stress that it describes the overall optical response of any graphene-assisted cavity. Note that, due to the cubic term (in turn produced by the graphene nonlinearity), \tilde{T} is generally a multi-valued function of W it assuming three different values within the shadowed region of Fig.2a. In Fig.2b we plot a portion of the region M (which is actually unbounded toward $Re(W) \rightarrow -\infty$) of the complex plane W on which the system transmittance is multi-valued. Therefore, we conclude that the system supports a strong nonlinear regime with a multi-valued transmittance whenever it is excited in such a way that W is in M .

The values of W belonging to the region M select the cavities actually hosting the predicted strong nonlinear regime and such region M allows the underlying physical supporting mechanism to be highlighted. The key observation is that the absolute value $|W|$ on the region M of

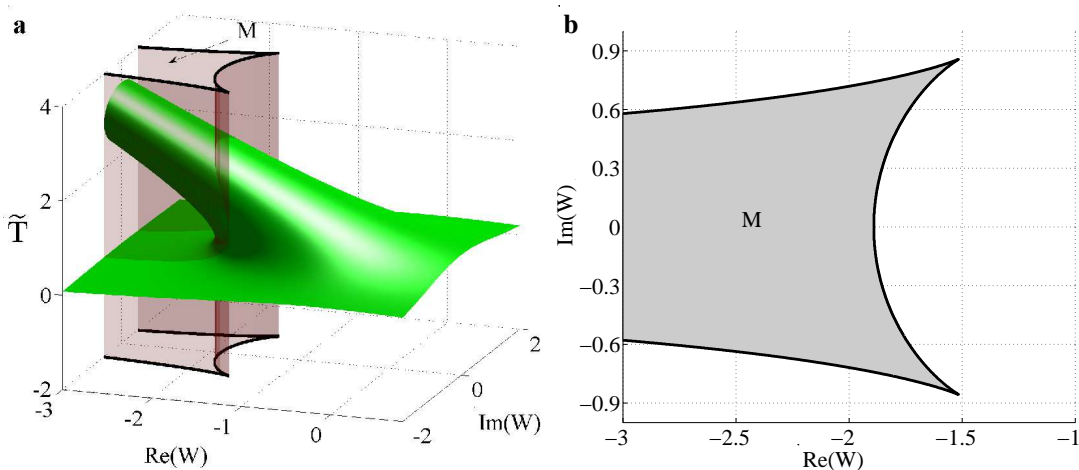


FIG. 2: **Conditions for the strong nonlinear regime supported by the graphene-assisted cavity.** (a) Modified cavity transmissivity \tilde{T} versus the complex parameter W characterizing the cavity status and excitation, showing the occurrence of a strong nonlinear system behavior. Due to normalization, such surface characterizes any possible graphene-assisted cavity response. (b) Region M of the complex plane W where the transmissivity is multi-valued. As explained in the text this region physically corresponds to a cavity excited close to its lasing threshold.

Fig.2b is of the order of unity (at least in the relevant region around its right boundary) and this requirement has to be compared with the second of Eqs.(4). Note that, as a consequence of the weakness of the nonlinear cubic term in Eq.(1), $c\mu_0|\sigma_3||E_i|^2 \ll 1$ unless the incident optical intensities is so large to make Eq.(1) useless and, at the same time, to severely damage the structure through heating. Therefore, in order to trigger the strong nonlinear regime at feasible optical intensities, from the second of Eqs.(4) we conclude that, the necessary requirement is

$$\Psi \equiv \left| \frac{\Omega}{\Lambda} + \frac{1}{2}c\mu_0\sigma_1 \right| \ll 1. \quad (6)$$

Considering Eq.(3) we note that the condition in Eq.(6) would lead the transmissivity of the linear cavity to be greater than one and this can only occur if an energy supplying mechanism is present in the bulk, thus justifying our choice of a gain medium where embedding the graphene layer (see Fig.1a). Condition in Eq.(6) corresponds to an active cavity operating close to one of its lasing threshold and this clarifies the physical mechanism supporting the strong nonlinear regime. Indeed, close to the lasing threshold, the wave inside the cavity starting from the graphene plane ($z = 0^+$) makes a complete round trip and returns to the graphene plane ($z = 0^-$) with almost the same amplitude and phase so that nonlinearity localized on the graphene plane, being the only residual agent not compensated by the cavity, can fully rule the field dynamics. We refer to this mechanism as the baring of the graphene nonlinearity produced by the cavity close to a lasing threshold. A different but equivalent way of grasping the same mechanism is observing that in Eq.(2) the nonlinear term (containing σ_3) is generally negligible thus leading to cavity to exhibit the

linear response of Eq.(3). However, if condition in Eq.(6) holds, the linear contribution in the LHS of Eq.(3) is very small as well so that the other nonlinear term cannot be neglected with the result of producing a marked system nonlinear behavior. It is worth stressing that such strong nonlinear regime cannot be observed without graphene since the free cavity is a purely linear device and the localization of the nonlinearity on a single plane plays, as explained, a fundamental role.

Graphene nonlinearity baring at optical frequencies. We now discuss the predicted strong nonlinear regime in a realistic situation at optical frequencies. We consider a cavity whose mirrors are silver layers of thickness $d = 0.22 \mu m$ and whose gain slabs are filled by Rhodamine 6G (Rh6G)-doped polymethyl methacrylate (PMMA) of thicknesses $L = 0.7 \mu m$. The cavity is pumped by an inverting laser beam at a wavelength of $532 nm$. We have chosen $\lambda = 565 nm$ as the field wavelength since it is near to the gain peak [34]. The silver and PMMA permittivities are, at the considered field wavelength, $\epsilon_{Ag} = -11.9641 + 0.8310i$ and $\epsilon_{PM} = 2.2282$, respectively. The permittivity of the gain medium is given by $\epsilon_G = \epsilon_{PM} - i \frac{\lambda}{2\pi} \sqrt{\epsilon_{PM}} \frac{\sigma_e N_T}{1+I/I'_{se}} \frac{I_p/I_{sp}}{1+I_p/I_{sp}}$ [34] where I is the optical intensity within the medium bulk, I_p is the pump intensity, I_{sp} is the pump saturation intensity, $I'_{se} = I_{se}(1 + I_p/I_{sp})$ (where $I_{se} = 300 kW/cm^2$) is the field saturation intensity, $\sigma_e = 1.2 \times 10^{-16} cm^2$ is the emission cross section and N_T is concentration of the Rh6G molecules. We have chosen the strong pump saturation regime by setting $I_p/I_{sp} = 5000$ so that $\frac{I_p/I_{sp}}{1+I_p/I_{sp}} \simeq 1$ and $I'_{se} \simeq 1500 MW/cm^2$ which is a sufficiently high saturation intensity to self-consistently assume that $I/I'_{se} \ll 1$ (a condition we have *a-posteriori* checked, see below) and to express the permittivity of the gain medium as

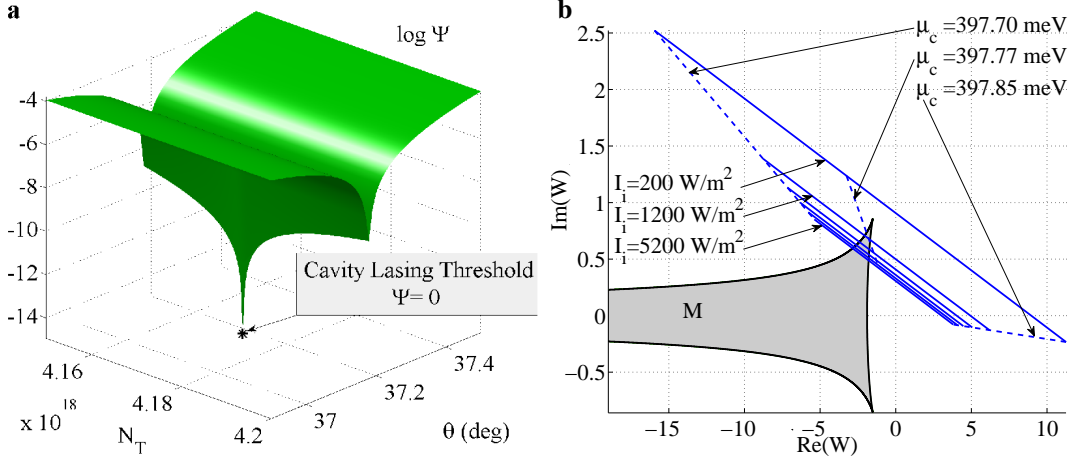


FIG. 3: **Cavity tuning and multi-valued response near the lasing threshold.** (a) Logarithmic plot of the function Ψ whose zeros correspond to the cavity lasing thresholds. In this example all the cavity parameters are held fixed except for the incidence angle θ and the concentration of the dye molecules N_T . The sharp peak corresponds to the cavity threshold. (b) The oblique solid lines represent the cavity states with fixed incident optical intensity I_i and varying chemical potential μ_c . Conversely the oblique dashed lines correspond to states whose μ_c is held fixed and whose I_i is varied. The shadowed region M is the same as in Fig.2b and it contains the states where the cavity response is multi-valued. The intersections of the solid lines with M prove that in the considered I_i and μ_c ranges the cavity actually shows a highly nonlinear behavior with multi-valued response features.

$$\epsilon_G = \epsilon_{PM} - i \frac{\lambda}{2\pi} \sqrt{\epsilon_{PM}} \sigma_e N_T.$$

As discussed in the above paragraph, Eq.(6) is the necessary requirement for observing the strong nonlinear regime. We have set $\mu_c = 400 \text{ meV}$ so that, using the expression for σ_1 (see Methods) and the above parameters, Ψ turns out to be a function of the incidence angle θ and the Rh6G molecules concentration N_T and the cavity lasing thresholds are the zeros of this function. In Fig.3a we draw the logarithmic plot of Ψ around one of its zeros which is located at $\theta = 37.1783 \text{ deg}$, $N_T = 4.1720 \times 10^{18} \text{ cm}^{-3}$. Note that, even though the region where $\Psi \ll 1$ is rather sharp in Fig.3a, the cavity threshold can be simply experimentally achieved by using a beam with small angular divergence around the predicted critical angle.

By slightly detuning the cavity from the lasing threshold, the highly nonlinear multi-valued behavior of the transmissivity appears. With all the above parameters fixed (except the chemical potential), we have chosen to investigate the system response for various chemical potentials in the range $397.7 \text{ meV} < \mu_c < 397.85 \text{ meV}$ (which are values sufficiently close to the above used $\mu_c = 400 \text{ meV}$) and various incident optical intensities $I_i = c\epsilon_0 |E_i|^2 / 2$ spanning the range $200 \text{ W/m}^2 < I_i < 5200 \text{ W/m}^2$. Using the expression for σ_3 (see Methods) we have evaluated the corresponding complex W parameters (see the second of Eqs.(4)) and we have plotted them on the complex plane in Fig.3b as oblique solid lines, each line corresponding to varying the chemical potential at a fixed incident intensity. In the same Fig.3b we have also reported the shadowed region M of Fig.2b (on a range of $\text{Re}(W)$ larger than that of Fig.2b) and, for complete-

ness, some oblique dashed lines each one corresponding to varying the incident intensity at a fixed chemical potential. The intersections of the solid oblique lines with the shadowed M region proves that on the considered ranges of μ_c and I_i the cavity actually shows a multi-valued behavior of the transmissivity.

In Figs.4a and 4b we have plotted the cavity transmissivity T and reflectivity $R = |E_r|^2 / |E_i|^2$ evaluated from Eq.(5) in the ranges of μ_c and I_i considered in Fig.3b. Note the multi-valued structures of both T and R which are the key feature of the above discussed strong nonlinear regime. It is also worth noting that such strongly nonlinear behavior occurs when the system is excited by ultra-low optical intensities of the order of $1000 \text{ W/m}^2 = 100 \text{ mW/cm}^2$ which are evidently small in comparison with those occurring in standard nonlinear optics.

In Figs.4c and 4d we report a comparison between the linear and the nonlinear cavity behavior. This is done by evaluating the cavity transmissivity and reflectivity at $I_i = 1 \text{ mW/m}^2$ (dashed lines) and $I_i = 5200 \text{ W/m}^2$ (solid lines). For $I_i = 1 \text{ mW/m}^2$ the effect of graphene nonlinearity is negligible so that dashed lines represent the linear graphene-assisted cavity response. It is worth noting that the discrepancy between linear and nonlinear behaviors is remarkable even for states at which the cavity response is not multi-valued (e.g on the range $397.755 \text{ meV} < \mu_c < 397.81 \text{ meV}$ on Figs.4c and 4d) so that the strong nonlinear regime occurs in a region larger than the M region of Figs.2b and 3b. In Fig.4c and 4d we also report the results of the full-wave simulations (see Methods) as dotted lines, performed to assure

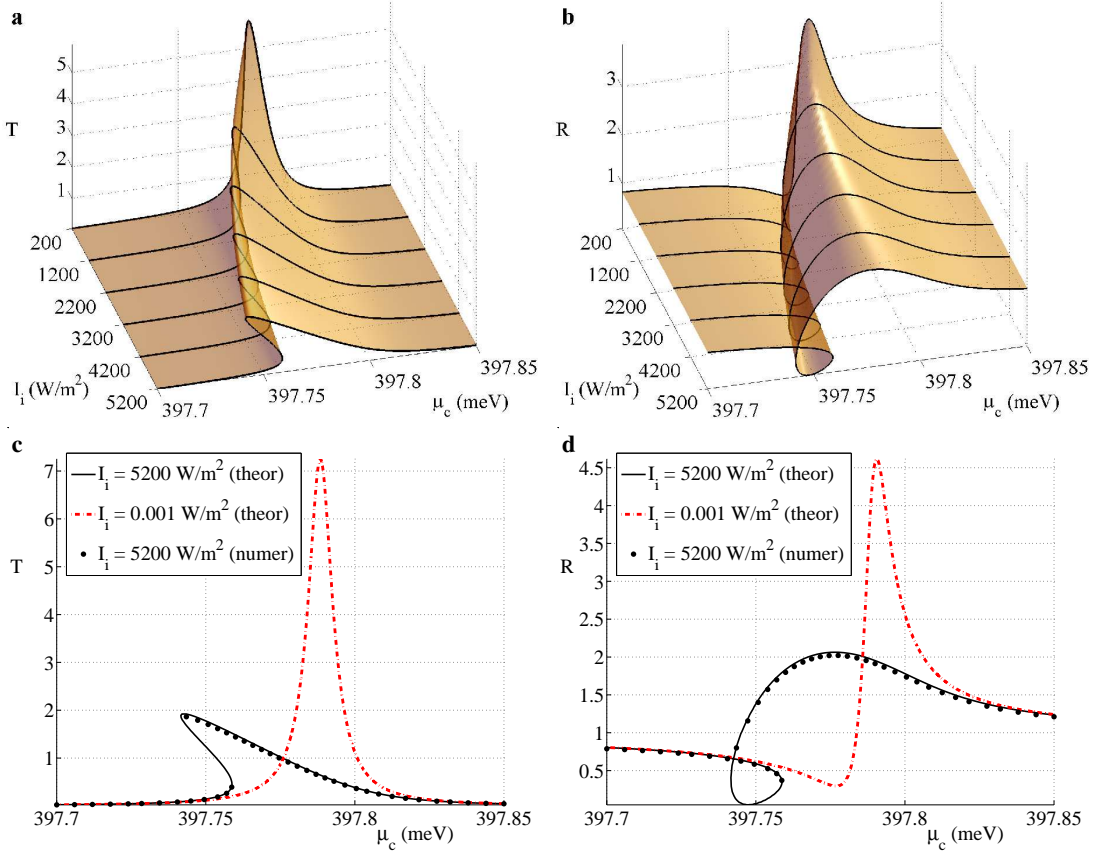


FIG. 4: **Nonlinear response of the graphene assisted cavity operating close to lasing threshold.** (a)(b) Cavity transmissivity T and reflectivity R plotted against the incident intensity I_i and the chemical potential μ_c . The solid lines on the surfaces correspond to T and R evaluated at the six incident intensities corresponding to the oblique solid lines of Fig.3b. The multivaluedness of both T and R is particularly evident and it occurs precisely at those (I_i, μ_c) states belonging to the intersection of the solid lines with the region M in Fig.3b. (c)(d) Comparison between the cavity transmissivity and reflectivity evaluated at $I_i = 5200$ W/m^2 (solid lines) and at $I_i = 1$ mW/m^2 (dashed lines). For $I_i = 1$ mW/m^2 the effect of graphene nonlinearity is negligible so that dashed lines represent the linear graphene-assisted cavity response. Note that a remarkable discrepancy between linear and nonlinear behavior also occurs on the range 397.76 $meV < \mu_c < 397.81$ meV where T and R are not multi-valued so that the strong nonlinear regime occurs in a region larger than the M region of Figs.2b and 3b. The results of the full-wave simulations are also plotted as dotted lines. The lower and upper branches of both T and R have been obtained by gradually increasing from $\mu_c = 397.7$ meV and decreasing from $\mu_c = 397.85$ meV the chemical potential, respectively.

stability of the predicted phenomenology. Specifically we have set $\mu_c = 397.7$ meV and have gradually increased this value, at each simulation using as initial guess the field profile obtained at the previous step. As a result we have obtained the lower branches of T and R as in Figs.4c and 4d, branches which stop at $\mu_c = 397.755$ meV where they bend upward. Analogously, as a second procedure, we have set $\mu_c = 397.85$ meV and gradually decreased this value with the same prescription of using the previous field profile as initial guess of each simulation. The upper branches of both T and R have been obtained and they stop at the value $\mu_c = 397.745$ meV . In addition to the evident agreement between theoretical and numerical predictions we stress that the adopted numerical route for achieving the different branches of T and R can in principle be used to experimentally prove the predicted bistability.

In Fig.5a we plot the real and imaginary parts of the electric field E_y within the cavity (see Methods) specific of the state $\mu_c = 397.76$ meV of Figs.4c and 4d. Note that, in addition to the evident field enhancement produced by the cavity (since for, $I_i = 5200$ W/m^2 , $E_i = 1.97 \cdot 10^3$ V/m), the electric field is practically left invariant by the reflection $z \rightarrow -z$ and this confirms our above reasoning that the field almost replicates itself after a complete round trip inside the cavity thus allowing the graphene nonlinearity on the plane $z = 0$ to strongly rule the cavity behavior. In Fig.5b we plot the optical intensity I within the cavity (see Methods) which, being much smaller than the above considered saturation intensity $I'_{se} \simeq 1500$ MW/cm^2 self-consistently assures that the model for the gain medium we have used is correct.

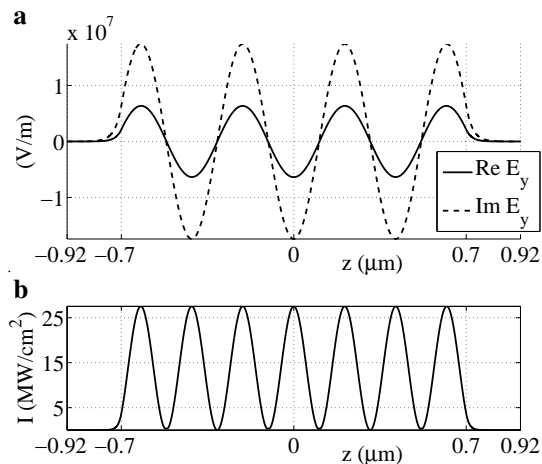


FIG. 5: **Cavity field profile and optical intensity.** (a) Real and imaginary parts of the electric field E_y within the cavity for the state $\mu_c = 397.76$ meV of Figs.4c and 4d. The field enhancement produced by the cavity is particularly evident since for, $I_i = 5200$ W/m², $E_i = 1.97 \cdot 10^3$ V/m. Note that, since the electric field is practically left invariant by the reflection $z \rightarrow -z$, the field almost replicates itself after a complete round trip inside the cavity, the fundamental physical ingredient allowing the considered strong nonlinear regime to occur. (b) Optical intensity I within the cavity corresponding to the situation of panel a. Note that such optical intensity is much smaller than the considered saturation intensity $I'_{se} \simeq 1500$ MW/cm² so that the model for the gain medium we have used is self-consistently correct.

II. DISCUSSION

A novel strategy has been proposed to fully exploit the graphene nonlinearity for achieving a very strong nonlinear regime. Specifically it has been suggested and theoretically proved that a standard cavity hosting an active medium, when excited close to its lasing threshold, is able to isolate the planar localized graphene nonlinearity as a consequence of the field replication after a round trip inside the cavity. Such a graphene nonlinearity baring turns the simple linear cavity into a highly nonlinear photonic device whose response is achievable at very low optical intensity and it has a marked multi-valued trait. Therefore, to the best of our knowledge, the proposed mechanism can also be placed among the first strategies to exploit graphene nonlinearity in bulk environment to achieve optical steering. A specific example has been considered at optical frequencies where all the above predicted features have been checked. It should be stressed that such example also highlights the efficiency of the proposed mechanism since, as it is well known, graphene nonlinearity at optical frequencies is much weaker than the remarkable one appearing in far infrared and terahertz ranges (note that very few graphene-based nonlinear optical setups have been proposed in literature). On the other hand, since suitable gain mechanism exist also at frequency lower than the optical ones,

the proposed graphene nonlinearity baring can in principle be exploited at such lower frequencies where an even stronger nonlinear regime is therefore expected. Among the possible applications of the considered setup it is worth stressing that the predicted bistable response of both cavity transmissivity and reflectivity can be exploited to conceive devices for optical information processing such as, evidently, optoelectronic memory units operating at low optical intensity.

III. METHODS

Linear and nonlinear graphene conductivities.

The surface conductivity of the graphene sheet, if $k_B T \ll |\mu_c|$, can be expressed as [33]

$$\sigma_1 = \frac{ie^2 k_B T}{\pi \hbar^2 (\omega + i2\Gamma)} \left(\frac{\mu_c}{k_B T} + 2 \ln \left(e^{-\frac{\mu_c}{k_B T}} + 1 \right) \right) + \frac{ie^2}{4\pi \hbar} \ln \left(\frac{2|\mu_c| - (\omega + i2\Gamma)\hbar}{2|\mu_c| + (\omega + i2\Gamma)\hbar} \right) \quad (7)$$

where e is the electron charge, \hbar and k_B are Planck's and Boltzmann's constant, respectively, T is the temperature which is here fixed at 300 K, μ_c is the graphene chemical potential and Γ is a phenomenological scattering rate accounting for the graphene intrinsic losses which is here fixed at $\Gamma = 0.43$ meV. The nonlinear conductivity coefficient σ_3 for graphene is given by [19, 25]

$$\sigma_3 = -i \frac{3}{32} \frac{e^4 V_F^2}{\pi \hbar^2 \omega^3 \mu} (1 + i\alpha_T) \quad (8)$$

where $V_F = 9.9 \times 10^5$ m/s is the Fermi velocity and $\alpha_T \approx 0.1$ is a phenomenological parameter accounting for two photon absorption in graphene.

Graphene-assisted cavity response. The field interacting with the cavity is transverse electric (TE) so that, with reference to Fig.1, it can be represented as $\mathbf{E} = e^{ik_0(\sin\theta)x} A_y(z) \hat{\mathbf{e}}_y$ and $\mathbf{H} = e^{ik_0(\sin\theta)x} [A_x(z) \hat{\mathbf{e}}_x + \sin\theta A_y(z) \hat{\mathbf{e}}_z] / (c\mu_0)$, where ω is the radiation frequency, $k_0 = \omega/c$ and A_x, A_y are the independent field components. In order to exploit the transfer matrix approach, it is convenient to introduce the two component column vector $A = (A_x \ A_y)^T$ for representing the field. The incident (i) and reflected (r) waves for $z < -d-L$ are $A_i = e^{ik_0 \cos\theta(z+d+L)} (-\cos\theta \ 1)^T E_i$, $A_r = e^{-ik_0 \cos\theta(z+d+L)} (\cos\theta \ 1)^T E_r$ whereas the transmitted wave for $z > d+L$ is $A_t = e^{ik_0 \cos\theta(z-d-L)} (-\cos\theta \ 1)^T E_t$, respectively. The connection between the fields incoming (in) and outgoing (out) from a homogeneous slab of thickness δ and dielectric permittivity ϵ is given by $A_{out} = M_{(K,\delta)} A_{in}$ where

$$M_{(K,\delta)} = \begin{pmatrix} \cos(K\delta) & -i(K/k_0) \sin(K\delta) \\ -i(k_0/K) \sin(K\delta) & \cos(K\delta) \end{pmatrix} \quad (9)$$

is the standard slab transfer matrix and $K = k_0\sqrt{\epsilon - \sin^2\theta}$. Therefore the fields at both sides of the graphene plane $z = 0$ are given by

$$\begin{aligned} \begin{pmatrix} A_x \\ A_y \end{pmatrix}_{z=0^-} &= M_{(K_G, L)} M_{(K_{Ag}, d)} \begin{pmatrix} \cos\theta(-E_i + E_r) \\ (E_i + E_r) \end{pmatrix}, \\ \begin{pmatrix} A_x \\ A_y \end{pmatrix}_{z=0^+} &= M_{(K_G, -L)} M_{(K_{Ag}, -d)} \begin{pmatrix} -\cos\theta E_t \\ E_t \end{pmatrix}. \end{aligned} \quad (10)$$

By setting the matching condition at the graphene plane $A_y^+ - A_y^- = 0$ and $A_x^+ - A_x^- = c\mu_0 K_y$ (where K_y is defined in Eq.(1) where $E_y = A_y^+ = A_y^-$), one obtains two equations containing E_i , E_r and E_t and the complex factor

$$\begin{aligned} \Omega &= \cos\theta \left[\cos(K_{Ag}d) \cos(K_G L) - \frac{K_G}{K_{Ag}} \sin(K_{Ag}d) \sin(K_G L) \right] \\ &\quad - i \left[\frac{K_{Ag}}{k_0} \sin(K_{Ag}d) \cos(K_G L) + \frac{K_G}{k_0} \cos(K_{Ag}d) \sin(K_G L) \right] \\ \Lambda &= \left[\cos(K_{Ag}d) \cos(K_G L) - \frac{K_{Ag}}{K_G} \sin(K_{Ag}d) \sin(K_G L) \right] \\ &\quad - i \cos\theta \left[\frac{k_0}{K_{Ag}} \sin(K_{Ag}d) \cos(K_G L) + \frac{k_0}{K_G} \cos(K_{Ag}d) \sin(K_G L) \right] \end{aligned} \quad (11)$$

By eliminating the amplitude E_r , Eq.(2) is readily obtained.

Once the amplitude E_t is evaluated from Eq.(2) at a given E_i (and hence also E_r is known), the above transfer matrix approach allows to evaluate the field in the cavity bulk. The optical intensity I within the cavity is the magnitude of the Poynting vector

$$\mathbf{S} = \frac{1}{2} \text{Re}(\mathbf{E} \times \mathbf{H}^*) = \frac{1}{2c\mu_0} \text{Re}[A_y(A_z^* \hat{\mathbf{e}}_x - A_x^* \hat{\mathbf{e}}_z)]. \quad (12)$$

Full-wave simulations. We have numerically evaluated the transmissivity and reflectivity of the considered TE mode in the optical cavity by resorting to the full-wave finite-element electromagnetic simulations (RF module, COMSOL). All the numerical simulations (whose results are reported in Figs.4c and 4d (dotted lines)) are carried out in the frequency domain and in 2D configuration. We have considered two vacuum layers placed at the facets of the silver slabs for providing optical external illumination and for evaluating transmission and reflection coefficients. We have adopted periodic boundary conditions along the x -axis imposing a Floquet phase shift boundary condition on the sides of the considered numerical domain. In addition, we have used matched boundary conditions at the entrance and exit facets (orthogonal to the z -axis) of the integration domain.

This research has been funded by the Italian Ministry of Research (MIUR) through the "Futuro in Ricerca" FIRB-grant PHOCOS - RBFR08E7VA.

-
- [1] Bonaccorso, F., Sun, Z., Hasan, T. and Ferrari, A. C. Graphene photonics and optoelectronics. *Nat. Photonics* **4**, 611-622 (2010).
- [2] Bao, Q. and Loh, K. P. Graphene Photonics, Plasmonics, and Broadband Optoelectronic Devices. *ACS Nano* **6**, 3677-3694 (2012).
- [3] Stauber, T., Peres, N. M. R., Geim, A. K. Optical conductivity of graphene in the visible region of the spectrum. *Phys. Rev. B* **78** 085432 (2008).
- [4] Bao, Q., Zhang, H., Wang, B., Ni, Z., Lim, C. H. Y. X., Wang, Y., Tang, D. Y., Loh, K. P. Broadband Graphene Polarizer. *Nat. Photonics* **5**, 411415 (2011)
- [5] Cheng, H., Chen, S., Yu, P., Li, J., Deng, Li., Tian, J. Mid-infrared tunable optical polarization converter composed of asymmetric graphene nanocrosses. *Opt. Lett.* **38**, 1567-1569 (2013).
- [6] Bludov Yu. V., Vasilevskiy M. I., Peres N. M. R. Tunable graphene-based polarizer. *J. Appl. Phys.* **112**, 084320 (2012).
- [7] Liu, M., Yin, X., Ulin-Avila, E., Geng, B., Zentgraf, T., Ju, L., Wang, F., Zhang, X. A graphene-based broadband optical modulator. *Nature* **474**, 64-67 (2011).
- [8] Sensale-Rodriguez, B., Yan, R. S., Kelly, M. M., Fang, T., Tahy, K., Hwang, W. S., Jena, D., Liu, L., Xing, H. G. Broadband graphene terahertz modulators enabled by intraband transitions. *Nat. Commun.* **3**, 780 (2012).
- [9] Gosciniak, J., Tan, D. T. H. Theoretical investigation of graphene-based photonic modulators. *Scientific Reports* **3**, 1897 (2013).
- [10] Gan, X., Shiue, R., Gao, Y., Mak, K. F., Yao, X., Li, L., Szep, A., Walker, D. Jr., Hone, J., Heinz, T. F., Englund, D. High-Contrast Electrooptic Modulation of a Photonic Crystal Nanocavity by Electrical Gating of Graphene. *Nano Lett.* **13**, 691-696 (2013).
- [11] Park, J., Ahn, Y., Ruiz-Vargas, C. Imaging of Photocurrent Generation and Collection in Single-Layer Graphene. *Nano Lett.* **9**, 17421746 (2009).
- [12] Xia, F., Mueller, T., Golizadeh-Mojarad, R., Freitag, M., Lin, Y., Tsang, J., Perebeinos, V., Avouris, P. Photocurrent Imaging and Efficient Photon Detection in a Graphene Transistor. *Nano Lett.* **9**, 10391044 (2009).
- [13] Mueller, T., Xia, F., Avouris, P. Graphene photodetectors for high-speed optical communications. *Nat. Photonics* **4**, 297-301 (2010).
- [14] Withers, F., Bointon, T. H., Craciun, M. F., Russo, S. All-Graphene Photodetectors. *ACS Nano* **7**, 50525057 (2013).
- [15] Bao, Q.L., Zhang, H., Wang, Y., Ni, Z.H., Yan, Y.L., Shen, Z.X., Loh, K.P., Tang, D.Y. Atomic-Layer Graphene as a Saturable Absorber for Ultrafast Pulsed Lasers. *Adv. Funct. Mater.* **19**, 30773083 (2009).
- [16] Xing, G., Guo, H., Zhang, X., Sum, T. C., Hon, C., Huan, A. The physics of ultrafast saturable absorption in graphene. *Opt. Express* **18**, 4564-4573 (2010).

- [17] Sun, Z. P., Hasan, T., Torrisi, F., Popa, D., Privitera, G., Wang, F. Q., Bonaccorso, F., Basko, D. M., Ferrari, A.C. Graphene Mode-Locked Ultrafast Laser ACS Nano **4**, 803-810 (2010).
- [18] Mikhailov, S. A. Non-linear electromagnetic response of graphene. Europhys. Lett. **79**, 27002 (2007).
- [19] Mikhailov, S. A., Ziegler, K. Nonlinear electromagnetic response of graphene: frequency multiplication and the self-consistent-field effects. J. Phys. Condens. Matter **38**, 384204 (2008).
- [20] Hendry, E., Hale, P. J., Moger, J., Savchenko, A. K., Mikhailov, S. A. Coherent Nonlinear Optical Response of Graphene. Phys. Rev. Lett. **105**, 097401 (2010).
- [21] Ishikawa, K. L. Nonlinear optical response of graphene in time domain. Phys. Rev. B **82**, 201402(R) (2010).
- [22] Zhang, H., Virally, S., Bao, Q., Ping, L. K., Massar, S., Godbout, N., Kockaert, P. Z-scan measurement of the nonlinear refractive index of graphene. Opt. Lett. **37**, 1856-1858 (2012).
- [23] Chen, W., Wang, G., Qin, S., Wang, C., Fang, J., Qi, J., Zhang, X., Wang, L., Jia, H., Chang, S. The nonlinear optical properties of coupling and decoupling graphene layers AIP Advances **3**, 042123 (2013).
- [24] Hong, S., Dadap, J. I., Petrone, N., Yeh, P., Hone, J., Osgood, R. M. Jr. Optical Third-Harmonic Generation in Graphene. Phys. Rev. X **3**, 021014 (2013).
- [25] Gorbach, A. V. Nonlinear graphene plasmonics: Amplitude equation for surface plasmons. Phys. Rev. A, **87**, 013830 (2013).
- [26] Auditore, A., De Angelis, C., Locatelli, A., Boscolo, S., Midrio, M., Romagnoli, M., Capobianco, A. D., Nallessio, G. Graphene sustained nonlinear modes in dielectric waveguides. Opt. Lett. **38**, 631-633 (2013).
- [27] Gorbach, A. V., Marini, A., Skryabin, D. V. Graphene-clad tapered fiber: effective nonlinearity and propagation losses. Opt. Lett. **38**, 5244-5246 (2013).
- [28] Gan, X., Mak, K. F., Gao, Y., You, Y., Hatami, F., Hone, J., Heinz, T. F., Englund, D. Strong Enhancement of Light-Matter Interaction in Graphene Coupled to a Photonic Crystal Nanocavity. Nano Lett. **12**, 5626-5631 (2012).
- [29] Thongrattanasiri, S., Garcia de Abajo, F. J. Optical Field Enhancement by Strong Plasmon Interaction in Graphene Nanostructures. Phys. Rev. Lett. **110**, 187401 (2013).
- [30] Gu, T., Petrone, N., McMillan, J. F., van der Zande, A., Yu, M., Lo, G. Q., Kwong, D. L., Hone, J., Wong, C. W. Regenerative oscillation and four-wave mixing in graphene optoelectronics. Nat. Photonics **6**, 554-559 (2012).
- [31] Furchi, M., Urich, A., Pospischil, A., Lilley, G., Unterrainer, K., Detz, H., Klang, P., Andrews, A. M., Schrenk, W., Strasser, G., Mueller, T. Microcavity-Integrated Graphene Photodetector. Nano Lett. **12**, 2773-2777 (2012).
- [32] Engel, M., Steiner, M., Lombardo, A., Ferrari, A. C., Lhneysen, H. v., Avouris, P., Krupke, R. Light-matter interaction in a microcavity-controlled graphene transistor. Nature Commun. **3**, 906 (2012).
- [33] Hanson, G. W. Dyadic Green's functions and guided surface waves for a surface conductivity model of graphene. Journ. Appl. Phys. **103**, 064302 (2008).
- [34] Soan, P. J., Case, A. D., Damzen, M. J., Hutchinson, M. H. R. High-reflectivity four-wave mixing by saturable gain in Rhodamine 6G dye. Opt. Lett. **17**, 781-782 (1992).